

Article

In-Situ Hydrogen Charging Effect on the Fracture Behaviour of 42CrMo4 Steel Submitted to Various Quenched and Tempering Heat Treatments

Atif Imdad * and Francisco Javier Belzunce Varela

Department of Materials Science and Metallurgical Engineering, University of Oviedo, 33203 Oviedo, Asturias, Spain

* Correspondence: uo256361@uniovi.es

Abstract: Research into safer, durable steels to be used in hydrogen-rich environments has been gaining importance in recent years. In this work, 42CrMo4 steel was subjected to quenched and tempered heat treatments using different temperature and time durations, in order to obtain different tempered martensite microstructures. Tensile tests on smooth and notched specimens were then performed in the air as well as with in situ electrochemical hydrogen charging using two different hydrogenated conditions. The harmful effects of hydrogen are more evident in tensile tests performed on notched specimens. The harder (stronger) the steel, the more hydrogen embrittlement occurs. As the steel's internal local hydrogen concentration rises, its strength must be gradually reduced in order to choose the best steel. The observed embrittlement differences are explained by modifications in the operative failure micromechanisms. These change from ductile (microvoid coalescence) in the absence of hydrogen, or under low hydrogen levels in the case of the softest steels, to brittle (cleavage or even intergranular fracture) under the most severe conditions.

Keywords: heat treatments; in-situ hydrogen charging; hydrogen embrittlement; structural steels



Citation: Imdad, A.; Varela, F.J.B. In-Situ Hydrogen Charging Effect on the Fracture Behaviour of 42CrMo4 Steel Submitted to Various Quenched and Tempering Heat Treatments. *Hydrogen* **2023**, *4*, 1035–1050. <https://doi.org/10.3390/hydrogen4040060>

Academic Editors: Pasquale Cavaliere and Geoffrey Brooks

Received: 4 November 2023

Revised: 4 December 2023

Accepted: 6 December 2023

Published: 11 December 2023



Copyright: © 2023 by the authors. Licensee MDPI, Basel, Switzerland. This article is an open access article distributed under the terms and conditions of the Creative Commons Attribution (CC BY) license (<https://creativecommons.org/licenses/by/4.0/>).

1. Introduction

Hydrogen's versatility, along with its zero carbon emissions, make it an ideal energy vector for future energy systems [1]. Extensive study has been conducted over the last two decades into the development of systems and equipment for the generation and storage of gaseous hydrogen and for the conversion of hydrogen into other kinds of energy. Significant breakthroughs, including increased efficiency and reduced costs, have been made [2]. In recent years, there has been a general interest in researching new materials that could carry and store hydrogen safely [3]. In order to mitigate hydrogen embrittlement and better understand how hydrogen influences the mechanical characteristics of medium- and high-strength steels, several investigations have been conducted of these materials [4,5].

The accumulation of hydrogen in specific microstructural areas, such as grain boundaries and other internal interfaces, results in hydrogen embrittlement (HE) during processing and fabrication (casting, chemical cleaning, pickling, electroplating, electrochemical machining, and welding). The entrance of atomic hydrogen into the crystalline network in metallic alloys usually reduces ductility, decreases fracture toughness, and increases the rate of crack growth under cyclic loads [6,7]. HE then produces failure at lower mechanical stresses by reducing the cohesive resistance of the internal surfaces.

The effects of hydrogen on metallic materials have been extensively studied, although the fundamental mechanics still remain unclear. The steel's strength and the amount of internal hydrogen are important features in hydrogen embrittlement failures. Usually, they are brittle failures, with cleavage or intergranular fracture micromechanisms. Failures caused by hydrogen have been linked to a variety of potential micromechanisms. The most well-known are hydrogen-induced decohesion (HEDE) [8,9] and hydrogen-enhanced

localized plasticity (HELP) [10,11]. Most recently, the HELP-mediated HEDE theory demonstrated the synergistic action of both micromechanisms [12,13]. The absorption of hydrogen into the steel, the atomic diffusion along its crystalline network, and the microstructure of the steel with different hydrogen traps are key aspects of these processes.

Among the many works dealing with the negative impact of hydrogen on the tensile properties of structural steels is the CHMC1-2014 standard published by the Canadian Standard Association, which evaluates the hydrogen compatibility and the suitability of materials to hydrogen services. It provides hydrogen embrittlement indexes (HEI) related to the reduction in area and notch tensile strength in slow-strain rate tensile tests carried out with smooth and notched specimens. Materials with HEI < 10% are considered appropriate for hydrogen services, whereas those with HEI > 50% are denoted as unsuitable [14]. The rest of the materials are subjected to hydrogen embrittlement and must be tested for fatigue crack growth rate and fracture toughness in gaseous hydrogen.

Regarding tensile properties, different authors have demonstrated that the hydrogen effect in steels is mainly reflected in ductility reductions (elongation and reduction in area), with yield strength and ultimate tensile strength remaining practically unaffected [15,16]. Nevertheless, the presence of hydrogen can even reduce the steel tensile strength in the case of high-strength steels or when tests are performed under high hydrogen levels [7,17]. On the other hand, there is broad agreement about how hydrogen affects the tensile behaviour of steels with notches: the presence of a stress concentrator may greatly lower both ductility and strength [17]. Zafra et al. [18] investigated the impact of tempering temperature on 42CrMo4 steel's susceptibility to hydrogen embrittlement using smooth and notched tensile specimens pre-charged with gaseous hydrogen. The embrittlement indexes increase with steel hardness, which is consistent with changes observed in their corresponding fracture micromechanisms. Zafra et al. [19] used 42CrMo4 hydrogen pre-charged specimens quenched and tempered at 600 °C for different times to show a linear reduction in fracture toughness as a result of the internal hydrogen that is present when the steel's yield strength increases. Wang et al. [17] demonstrated that hydrogen embrittlement increases with the stress concentration factor in notched tensile tests performed on high-strength quenched and tempered 34CrMo4 steel. Higher hydrostatic stresses are produced ahead of the notch due to the existence of a larger stress concentration factor. As a result, hydrogen atoms accumulate in that location, increasing the local hydrogen concentration and lowering the stress needed to fracture the specimen. Hydrogen embrittlement increases with the steel yield strength because the hydrostatic stress level also increases [20,21]. Imdad et al. [22] studied the effect of in situ electrochemical hydrogen charging on 42CrMo4 steel submitted to annealed, normalised, and quenched and tempering heat treatments at different temperatures using notched tensile specimens, showing substantial degrees of plastic deformation in the notch tip region, causing a high accumulation of hydrogen in the processing zone, which results in significant reduction in strength.

The main goal of this research is to investigate how different tempering temperatures and times affect the embrittlement of smooth and notched tensile specimens of 42CrMo4 steel tested while hydrogen is electrochemically introduced (in situ hydrogen charging). In this case, hydrogen enters the specimen at the same time as it is loaded, while its surface is plastically deformed (as also occurs in defects present in pipes and vessels in contact with hydrogen). In general, it was observed that the strength of the steel decreases as the local hydrogen concentration in the process zone increases and the operative failure micromechanisms are modified from microvoids' coalescence in all tests performed in air, to quasi-cleavage in tests with the simultaneous entrance of hydrogen. Intergranular failures were also observed in notched tensile specimens performed with grades with the greatest hardness and yield strength.

2. Materials and Experimental Methods

2.1. Heat Treatments

The chemical composition of the 42CrMo4 steel used in the present work is shown in Table 1. Because of its strength, hardness, and fatigue resistance, this steel is frequently employed in high-pressure hydrogen environments [19].

Table 1. 42CrMo4 steel's chemical composition (weight percent).

C%	Cr%	Mo%	Mn%	P%	S%
0.42	0.98	0.22	0.62	0.008	0.002

The steel was delivered as a hot-rolled plate with dimensions of 250 mm in length, 250 mm in width, and 12 mm in thickness. The steel was submitted to the quenching and tempering treatments described in Table 2 to produce tempered martensite microstructures (Q + T). All samples were quenched from 845 °C and tempered at 600 °C for different tempering times, ranging from a very small time (3 min) to a very long time (24 h). Additionally, a completely tempered microstructure (725 °C for 4 h) was also produced.

Table 2. Heat treatments: WQ = water-quenched and T = tempered.

Steel Grade	Heat Treatment
QT600-3m	845 °C/40 min + WQ + 600 °C/3 min tempered
QT600-30m	845 °C/40 min + WQ + 600 °C/30 min tempered
QT600-2h	845 °C/40 min + WQ + 600 °C/2 h tempered
QT600-24h	845 °C/40 min + WQ + 600 °C/24 h tempered
QT725-4h	845 °C/40 min + WQ + 725 °C/4 h tempered

Vickers hardness testing was performed with a 32 kg load applied for 15 s.

2.2. Tensile Tests

According to ISO 6892-1:2017 [23], tensile tests were performed on cylindrical, smooth and circumferentially notched specimens, whose geometries and dimensions are shown in Figure 1. An Instron 5582 tensile testing equipment was used for the experiments. The notch cross-section radius was 2.5 mm, and the notch depth and radius were 2 mm and 0.2 mm, respectively. The notched specimen's stress concentration factor, kt , was 3.71 [24].

Testing Conditions

Tensile specimens with notches and smooth surfaces were tested under three different conditions. The first test was always conducted at a standard displacement rate of 0.4 mm/min in air at room temperature without hydrogen, according to current standards. The remaining two criterions involved testing with external hydrogen using in situ electrochemical hydrogen charging. Conditions with relatively low hydrogenation were created with an acidic 1 M H₂SO₄ solution and a current density of 1 mA/cm². On the other hand, utilizing the same acidic solution and 0.25 g/L of As₂O₃, together with a current density of 0.5 mA/cm², resulted in a strongly hydrogenated situation. As₂O₃ was added to prevent hydrogen atoms from recombining, which increases hydrogen entry. Under these low and high hydrogen-charging conditions, the same steel (quenched and tempered at 700 °C for two hours, with a hardness of 223 HV) was saturated with hydrogen at concentrations of 0.5 and 0.95 ppm, respectively [25]. In the former, a typical high-pressure hydrogen service is represented, while in the latter, the steel is exposed to approximately twice as much hydrogen.

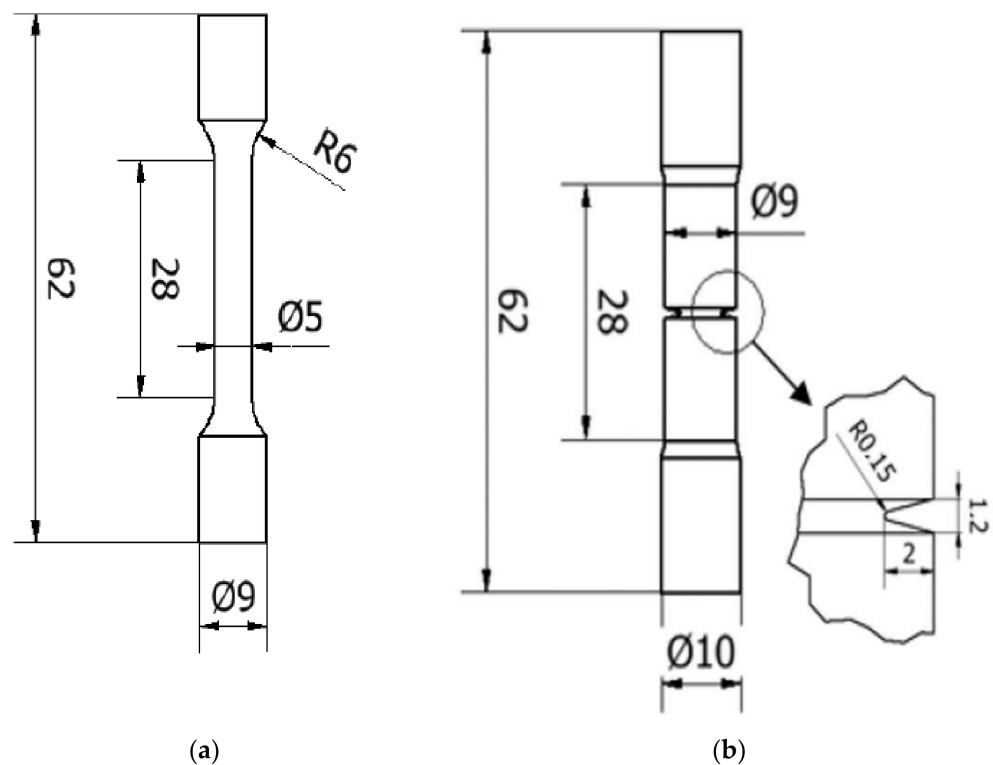


Figure 1. Geometry and dimensions of specimens: (a) smooth tensile; (b) notched tensile specimens.

The displacement rate used for all in situ hydrogen-charged testing was extremely low, at 0.01 mm/min. As room temperature, the hydrogen diffusion coefficients of these steels varied between $3.43 \times 10^{-11} \text{ m}^2/\text{s}$, in the case of the grade tempered for the shortest time (QT600-3m), and $1.43 \times 10^{-10} \text{ m}^2/\text{s}$ for the fully tempered grade (QT725-4h) [26]. Sufficient time for hydrogen to diffuse and accumulate in the process zone was provided, thus maximizing hydrogen embrittlement under the tested conditions. The applied load and the specimen elongation were continuously logged. Yield strength, σ_{ys} , ultimate tensile strength (σ_{ts}), tensile elongation (e), and reduction in area (RA) were measured for the smooth tensile tests. In case of the notched specimen, the maximum recorded tensile load was divided by the initial cross-sectional area at the notch (with a nominal diameter of 5 mm), as shown in Figure 1b, to obtain the ultimate strength at failure, σ_{NS} , with the notched specimens. In general, only one test was performed per condition, with tests being repeated when any signs of inconsistency were observed. The obtained results were consistent enough.

The hydrogen embrittlement index (HEI) was used to quantify the degree of hydrogen embrittlement. The HEI ranges between 0% (no embrittlement; $X_H = X$) and 100% (maximum possible hydrogen embrittlement; $X_H = 0$):

$$\text{HEI}\% = \frac{X - X_H}{X} \cdot 100$$

where X_H and X are the obtained steel properties, measured with and without hydrogen, respectively.

3. Results and Discussion

3.1. Microstructure

The SEM microstructures of all these samples are presented in Figure 2. They all are tempered martensite. The steel grade that was tempered at 600 °C for a very short time (3 min) was barely tempered (although some carbides had already precipitated, Figure 2a), and had high hardness (484 HV). After tempering at 725 °C for 4 h a fully tempered

microstructure, the lowest hardness (206 HV) was attained, as shown in Figure 2e. Carbide morphology and size are strongly modified during tempering. Initially, elongated carbides precipitate at the borders of martensitic laths, packs, or blocks. However, when tempering time or temperature increase, these carbides fragment, grow, and eventually globulize, producing a more uniform distribution. Dislocation density and martensite acicularity both concurrently decrease, relaxing the martensitic structure [20].

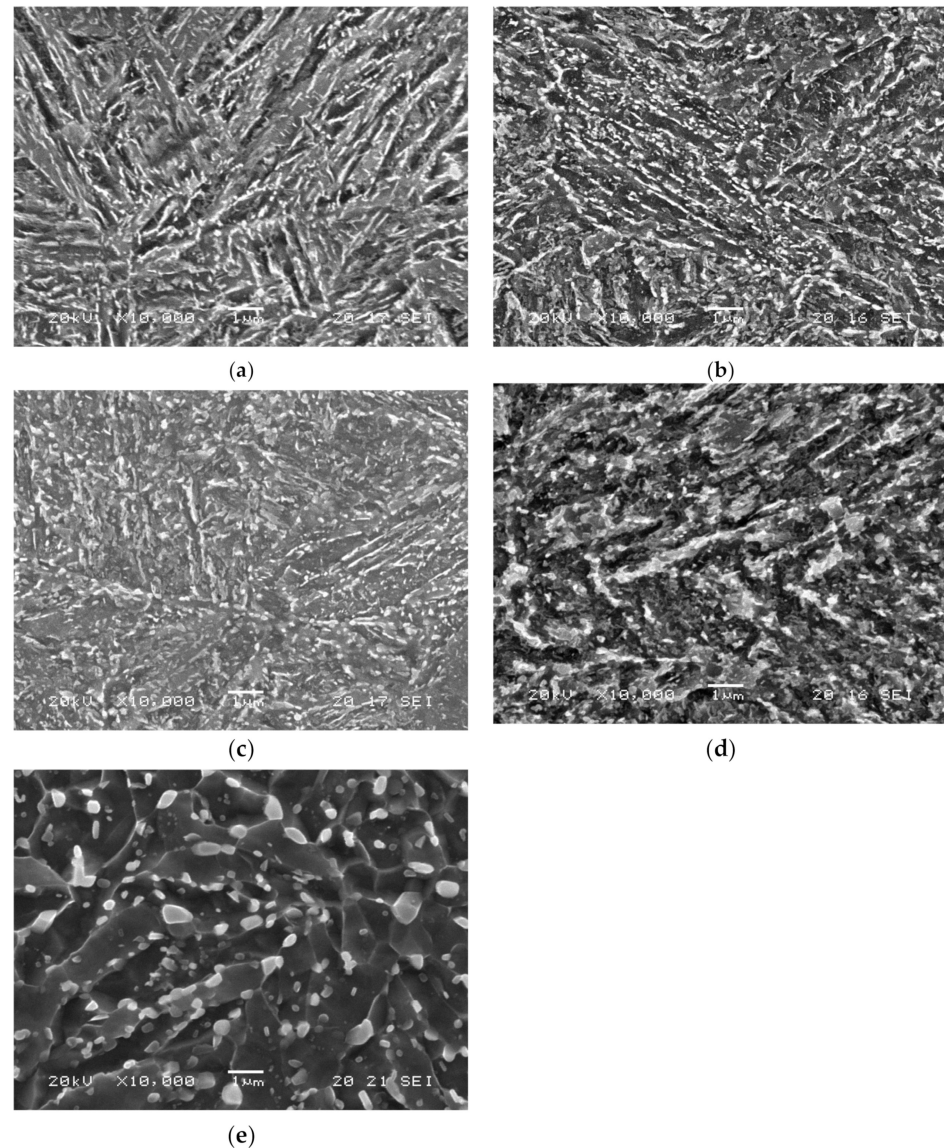


Figure 2. 42CrMo4 microstructures of (a) QT600-3m, (b) QT600-30m, (c) QT600-2h, (d) QT600-24h, and (e) QT725-4h at magnification $\times 10,000$.

The effect of tempering is better shown, representing the hardness versus the tempering parameter, which considers both temperature and time, with T expressed in K and time in hours:

$$P = T (20 + \log t)$$

Figure 3 shows the linear connection between the tempering parameter and hardness.

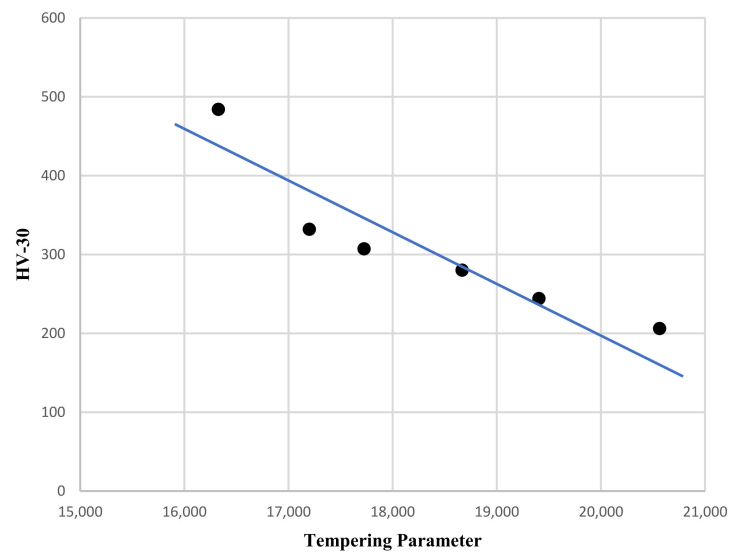


Figure 3. HV30 hardness versus tempering parameter.

3.2. Tensile Results and Failure Analysis

3.2.1. Smooth Tensile Test Results

Table 3 shows the tensile test results obtained with smooth tensile specimens, including displacement rate, yield, and ultimate strengths, σ_{ys} and σ_{ut} , as well as embrittlement indexes related to the ultimate tensile strength and reduction in area (RA).

Table 3. Smooth tensile test results. Tests in air and under low- and high-hydrogenation conditions.

Steel Grade	Hardness	Test Conditions	Displacement Rate (mm/min)	σ_{ys} (MPa)	σ_{ts} (MPa)	HEI (σ_{ts}) (%)	HEI (RA) (%)
QT600-3m	484 HV	air	0.4	1585	1770	--	--
		low H	0.01	--	865	51	100
		high H	0.01	--	365	79	100
QT600-30m	332 HV	air	0.4	1119	1204	--	--
		low H	0.01	1094	1094	9	65
		high H	0.01	1079	1079	10	70
QT600-2h	307 HV	air	0.4	910	1002	--	--
		low H	0.01	923	956	4.6	70
		high H	0.01	842	919	8.3	80
QT600-24h	280 HV	air	0.4	796	884	--	--
		low H	0.01	780	866	2	74
		high H	0.01	765	844	4.5	80
QT725-4h	206 HV	air	0.4	526	607	--	--
		low H	0.01	564	608	0	63
		high H	0.01	598	644	0	83

Figure 4 shows the stress–strain plots recorded with these grades. The sample quenched and tempered for only three minutes at 600 °C, with a hardness of 484 HV, was fully embrittled in both hydrogen environments, with failure taking place in the elastic region, well below the yield strength obtained in the hydrogen-free test (Figure 4a). The corresponding ultimate tensile strength suffered huge reductions: 51% without and 79% with the arsenic oxide in the electrolyte. Maximum embrittlement indexes of 100% related to the reduction in area were obtained.

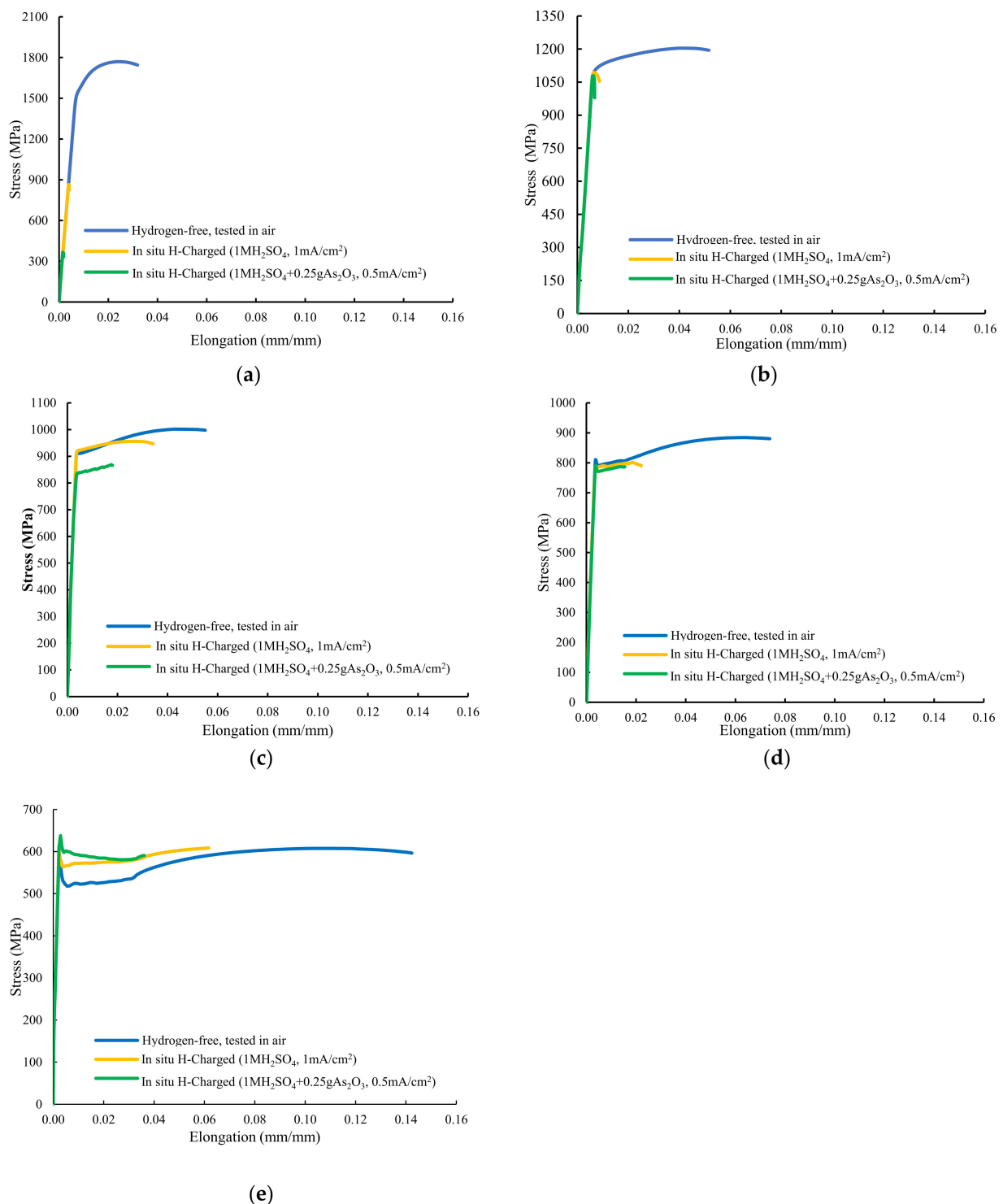


Figure 4. Stress–strain curves of smooth tensile tests performed on: (a) QT600-3m, (b) QT600-30m, (c) QT600-2h, (d) QT600-24h, and (e) QT725-4h.

In both hydrogenated conditions, with the sample tempered at 600 °C for 30 min (Figure 4b), failure only occurred at the end of the elastic region, with no plastic deformation. High hydrogen embrittlement indexes related to reduction in area were again observed in this grade (65% and 70%). Nevertheless, HEIs related to the strength were low (9–10%). Samples tempered at 600 °C for 2 h and 24 h suffered some plastic deformation before failure in both hydrogenated media (Figure 4c,d). A marked reduction in area was detected in tests with simultaneous hydrogen charging. Finally, Figure 4e shows the stress–strain

plot of the sample tempered at 725 °C for 4 h. An increase in the yield strength was detected (solid solution hardening due to hydrogen) but, even with this low-hardness, fully tempered microstructure, high hydrogen embrittlement indexes related to reduction in area were calculated in both hydrogen media (63% and 83%).

Figure 5a shows the failure surface of the grade with the highest hardness (QT600-3m) tested in air. It has a fully ductile behaviour: microvoids coalescence (MVC) was the only failure micromechanism that was observed. MVC was also observed in the rest of the tests performed in air (Figure 5b shows the grade with the lowest hardness, QT725-4h).

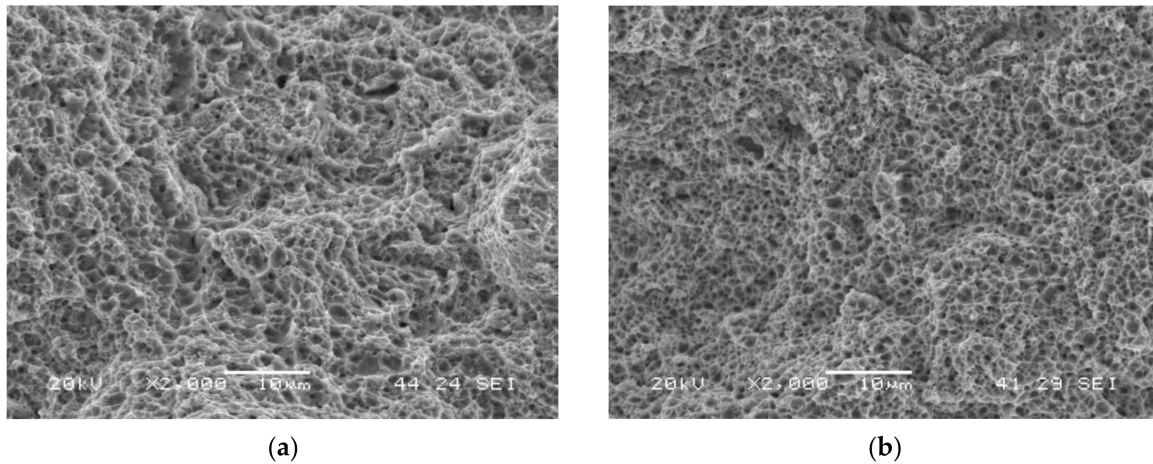


Figure 5. Failed surfaces of smooth tensile test specimens tested in air: (a) QT600-3m; (b) QT725-4h.

A notable change in the operative failure micromechanism took place when these grades were tested with simultaneous hydrogen charging. Quasi-cleavage (QC) was the main operative failure micromechanism in highly hydrogenated conditions, but intergranular failure (IG) was also observed in the grade with the highest hardness, tempered for the shortest time: QT600-3m (Figure 6a). When the electrolyte without arsenic oxide was used, QC was also the operative failure micromechanism in most cases, but MVC was also observed in QT600-24h and QT725-4h steel grades (Figure 6c,d).

3.2.2. Notched Tensile Test Results

Table 4 shows the results of the notched tensile tests performed in air and under in situ hydrogen charging conditions. The grade with the highest hardness and strength exhibits exceptionally high embrittlement indexes (related to notch strength) under both hydrogenated conditions (77% and 78%). For the remaining grades, the HEI was similarly high, but it progressively dropped as the temperature and tempering time increased and hardness decreases. As more hydrogen is present in the solution containing arsenic oxide (high H), HEI was also consistently greater in this condition.

The stress–strain plots recorded in all these tests are presented in Figure 7. Extraordinary reductions in notched tensile strength were observed in the grades with the highest hardness, QT600-3m and QT600-30m, tested in both hydrogenated media, and also with QT600-2h when tested in highly hydrogenated medium (solution with As₂O₃), with HEI values of approximately or higher than 50%. Failure took place after low plastic deformations occurred in the rest of in situ hydrogen charged tests. Only the two grades with the lowest hardness (QT600-24h and QT725-4h) tested in the medium with low hydrogenation (without As₂O₃), with HEI indexes below 10%, can be regarded as suitable for hydrogen services according to CHMC1-2014 [14].

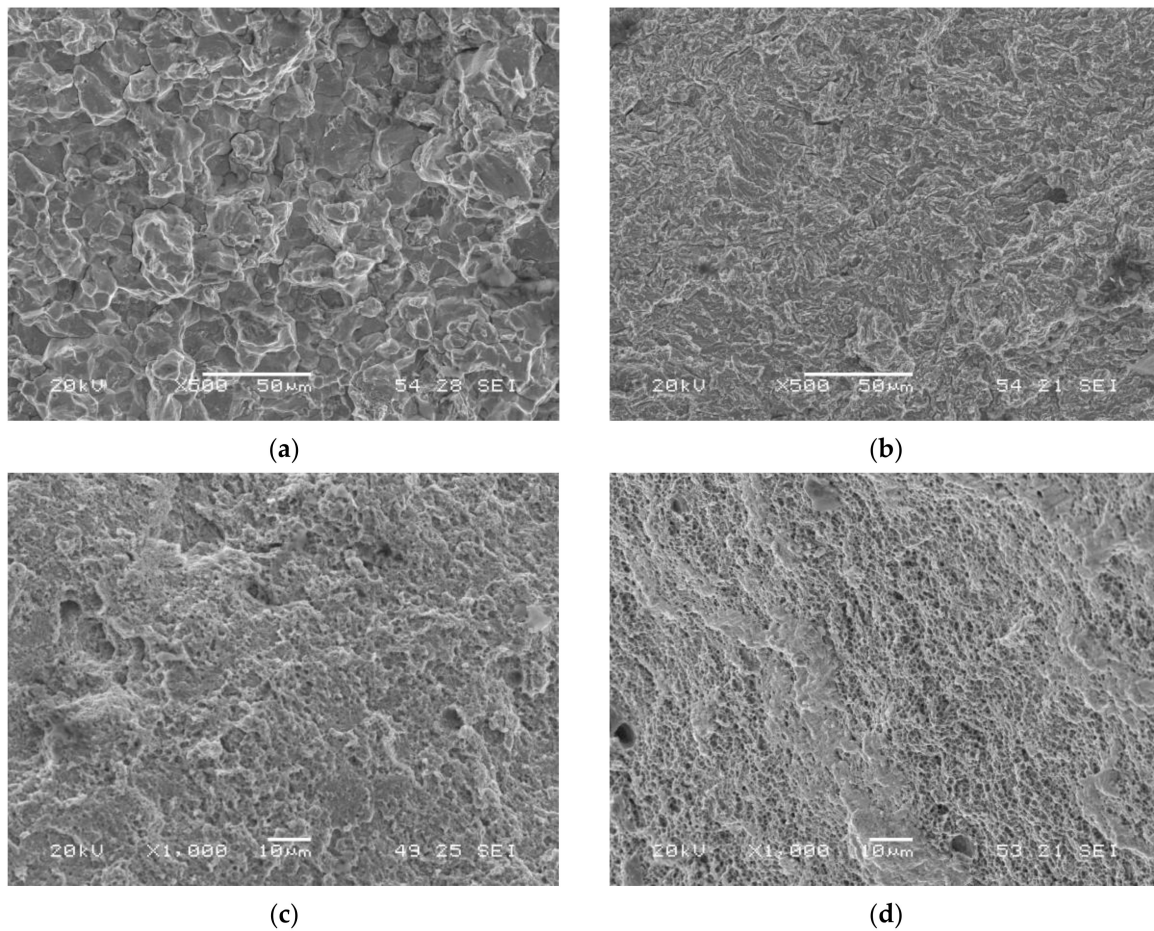


Figure 6. Failed surfaces of smooth tensile test specimens: (a) QT600-3m tested in the electrolyte with As_2O_3 ; (b) QT725-4h tested in the electrolyte with As_2O_3 ; (c) QT600-24h tested in the electrolyte without As_2O_3 ; (d) QT725-4h tested in the electrolyte without As_2O_3 .

Table 4. Notched tensile test results. Tests in air and in low- and high-hydrogenation conditions.

Steel Grade	Hardness	Test Conditions	Displacement Rate (mm/min)	σ_{NS} (MPa)	HEI (σ_{NS}) (%)
QT600-3m	484 HV	air	0.4	2055	--
		low H	0.01	476	77
		high H	0.01	457	78
QT600-30m	332 HV	air	0.4	1870	--
		low H	0.01	930	50
		high H	0.01	792	58
QT600-2h	307 HV	air	0.4	1701	--
		low H	0.01	1299	31
		high H	0.01	891	48
QT600-24h	280	air	0.4	1455	--
		low H	0.01	1306	10
		high H	0.01	1083	26
QT725-4h	206	air	0.4	1053	--
		low H	0.01	961	9
		high H	0.01	851	19

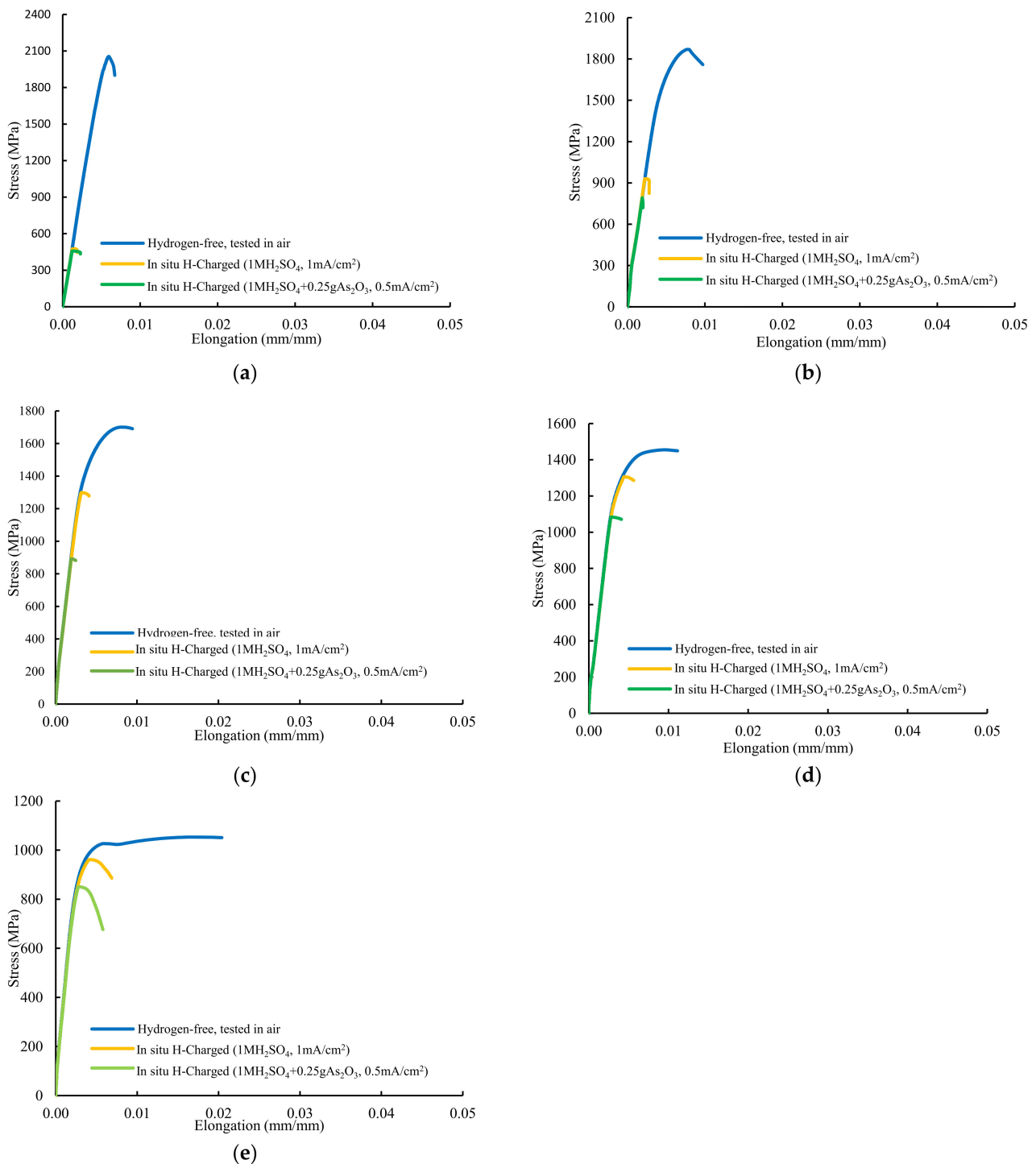


Figure 7. Stress–strain curves of notched tensile tests performed on: (a) QT600-3m, (b) QT600-30m, (c) QT600-2h, (d) QT600-24h, and (e) QT725-4h grade.

Microvoids' coalescence (MVC) was the failure micromechanism in all notched tensile test carried out in air, whereas quasi-cleavage (QC) and intergranular failure (IG) were seen in tests conducted in the two hydrogenated media. When the embrittlement index was greater than 50%, IG was visible, while QC was seen in the remaining grades. A few examples of these micromechanisms are displayed in Figure 8: IG in the sample with maximum hardness (QT600-3m) and QC in the fully tempered sample (QT725-4h). Figure 9a,b show the failed surface of QT600-30m tested in the two hydrogenated media.

A slight increase in the intergranular micromechanism is observed when the test was performed in the high-hydrogenated medium (with As_2O_3).

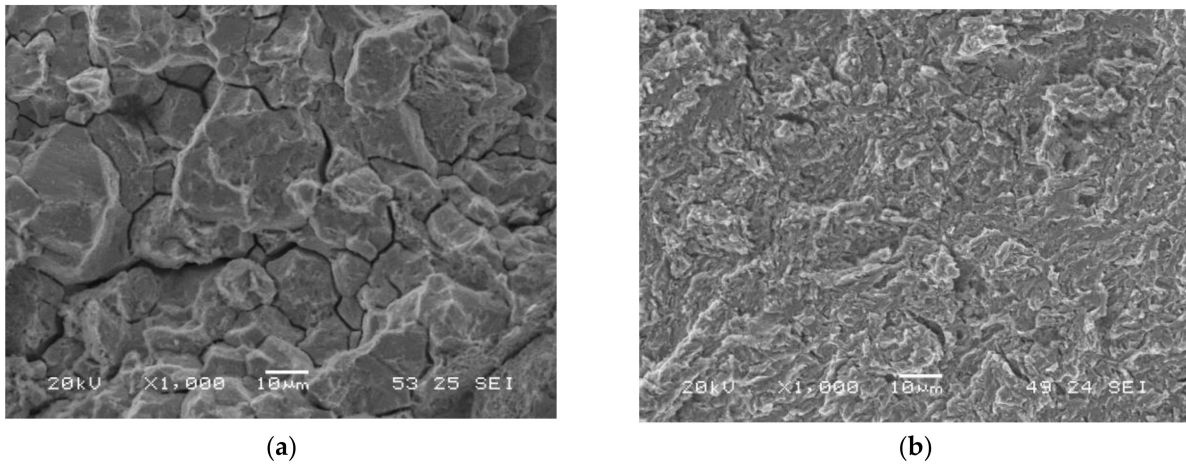


Figure 8. Failure micromechanisms observed on notched tensile test specimens with in situ hydrogen charged in the electrolyte without As_2O_3 : (a) QT600-3m; (b) QT725-4h.

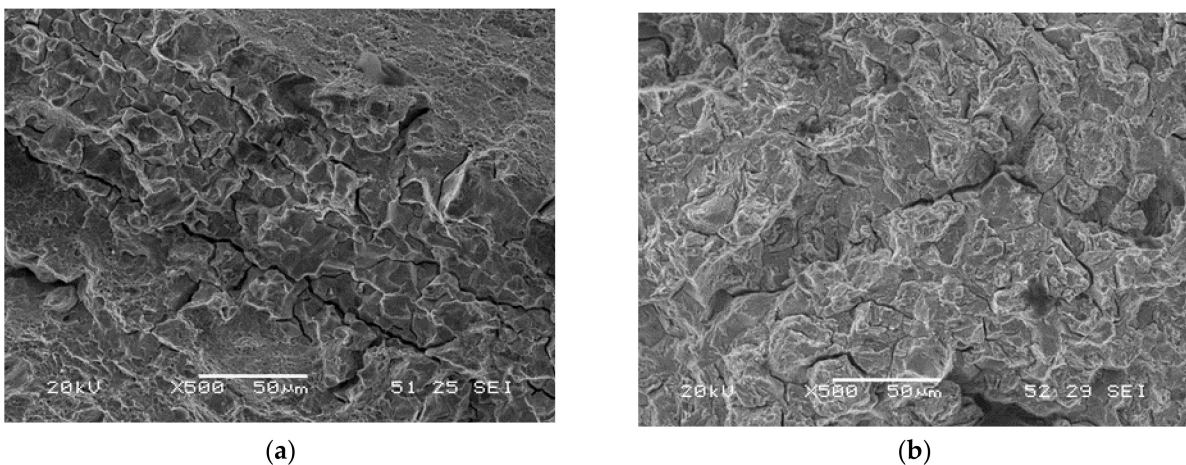


Figure 9. Failure micromechanisms observed on QT600-30m notched tensile test specimens with in situ hydrogen charged in: (a) the electrolyte without As_2O_3 ; (b) the electrolyte with As_2O_3 .

4. Discussion

The ultimate tensile strength values (σ_{ts}) for smooth tensile samples of all quenched and tempered (QT) grades evaluated in air, under low-hydrogenation (mild H), and strongly hydrogenated (high H) conditions are plotted against HV30 hardness in Figure 10. In all the tests performed in air (blue squares in Figure 10), the ultimate tensile strength is directly proportional to the steel's hardness: a greater hardness corresponds to higher tensile strength. The effect of hydrogen on the ultimate tensile strength measured in these grades is generally very low, with the exception of the significant decrease observed in the grade with the highest hardness (quenched and tempered for 3 min, 484 HV). Under both hydrogenated conditions, the highest ultimate tensile strength was obtained with the quenched grade tempered at 600 °C for 30 min (1094 and 1079 MPa under low and high hydrogen, respectively). Results in the same line were obtained by different authors using different steels and hydrogenated conditions (pre-charged specimens and gaseous hydrogen charging) [15,16,19].

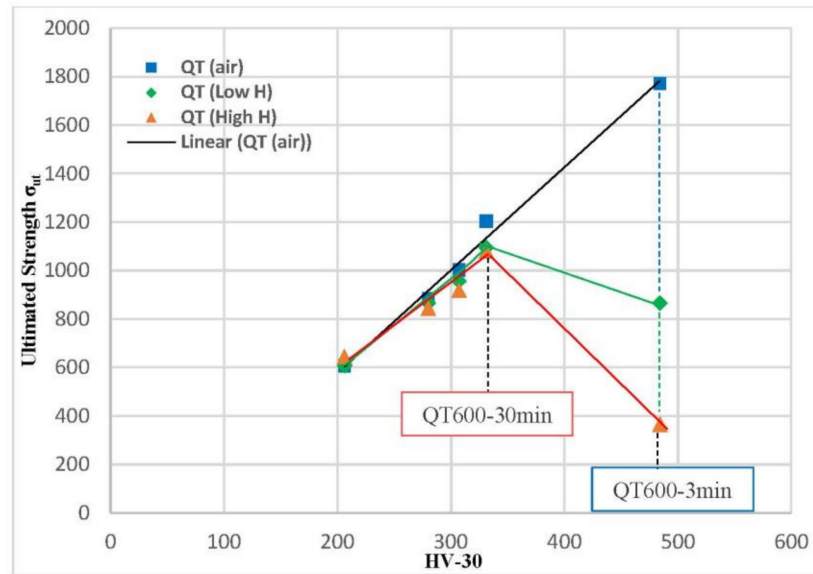


Figure 10. Ultimate tensile strength (σ_{ts}) versus HV30 hardness. Smooth tensile specimens of quenched and tempered 42CrMo4 grades tested in air and under in situ H charging.

The hydrogen embrittlement indexes related to the ultimate tensile strength (σ_{ts}) and reduction in area (RA) for the steels tested in low- and high-hydrogen conditions are displayed in Figure 11, as well as a comparison with their Vickers hardness. Except for the grade with the highest hardness, which was tempered for only three minutes, the embrittlement indexes related to the tensile strength are quite low (less than 15%). However, extremely significant embrittlement indexes, consistently exceeding 60% and 70%, were measured in the low and highly hydrogenated media, respectively, in relation to the reduction in area. In all cases, higher hydrogen embrittlement indexes were obtained with the medium that introduces more hydrogen (solution with arsenic oxide).

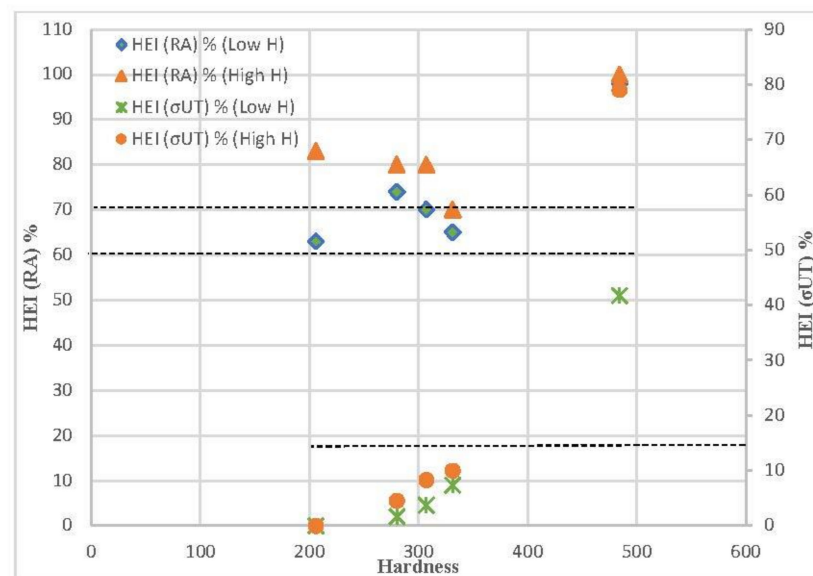


Figure 11. Influence of steel hardness on the hydrogen embrittlement indexes related to tensile strength and to reduction in area.

Because hydrogen enters, diffuses, and accumulates in the region directly ahead of the notch, hydrogen embrittlement is always greater when the stress concentrators (notched tensile specimens) are present, where a state of high hydrostatic stress is produced (high

triaxiality). Hydrogen atoms are attracted by the hydrostatic stress, σ_H , existing just ahead of the notch until an equilibrium hydrogen concentration, C_H , given by the following expression, is attained [27]:

$$C_H = C_0 \exp(\sigma_H V_H / RT)$$

where C_0 is the hydrogen concentration at zero stress and V_H is the partial molar volume of hydrogen, which can be approximated by $2 \times 10^{-6} \text{ m}^3/\text{molH}$ in a ferritic microstructure. The hydrogen diffusion distance from the tip of the notch, where hydrogen is entering the specimen, to the location the hydrostatic stress maximum just ahead of the notch was calculated by Zafra [28] to be between 0.1 and 0.2 mm.

The notched tensile strength was plotted versus the steel hardness in air and in both hydrogenated environments for various quenched and tempered microstructures in Figures 12 and 13. The greatest notched tensile strength in air is found in the hardest grade (484 HV, QT600-3m). Notched strength progressively reduces in these tests, as hardness does. In the tests of media with low hydrogenation, a dramatic decrease in the notched tensile strength is suffered by all grades with a hardness higher than 300 HV. The maximum value of the notched tensile strength was obtained with the grades quenched and tempered at 600 °C for 2 h (307 HV) and 24 h (280 HV), 1299 and 1306 Mpa, respectively. Zafra [17] also observed the same trend on the same steel using different tempering temperatures and specimens pre-charged in gaseous hydrogen at a high temperature.

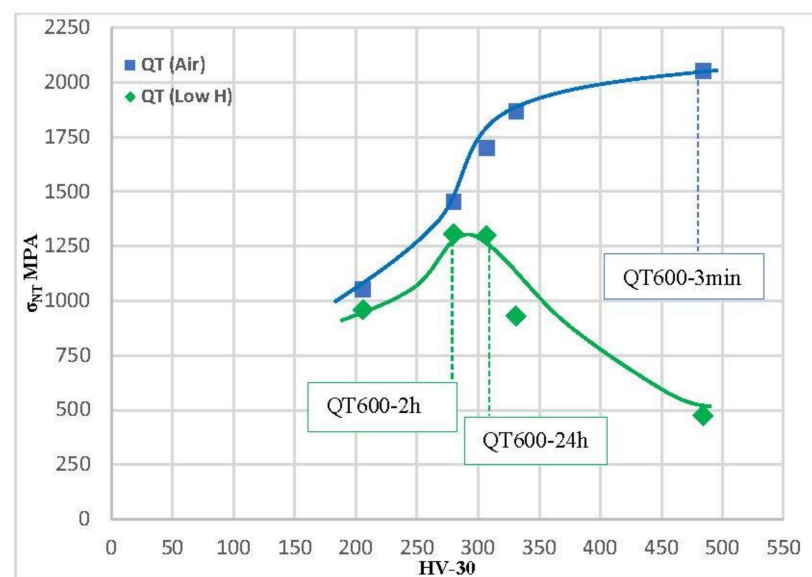


Figure 12. Tensile strength of notched steel in relation to steel hardness for all quenched and tempered grades evaluated under low-H and air conditions.

In the tests performed in highly hydrogenated medium, the effect of hydrogen is similar but even more dramatic. Very high decreases in notched tensile strength were observed in tests with electrochemical hydrogen charging in grades with a hardness higher than 275 HV. The maximum value of the notched tensile strength in these hydrogen conditions was obtained with the grades quenched and tempered at 600 °C for 24 h (1083 MPa).

Since yield strength is the characteristic that is usually used to evaluate hydrogen embrittlement and design structural components, Figure 14 plots the hydrogen embrittlement indexes that were obtained with all these grades in both high- and low-hydrogenated conditions against the yield strength of these steels. The quenched and tempered grades show a reasonably linear increase in these indexes along with the yield strength in both hydrogenated conditions. Changes in the operative failure micromechanism, from quasi-cleavage (QC) to intergranular failure (IG), justifies the increase in embrittlement with the steel yield strength. These two failure micromechanisms were also observed in most works

related to hydrogen embrittlement, and intergranular failure always corresponds to the most aggressive hydrogen conditions and larger embrittlement indices [17,18,22].

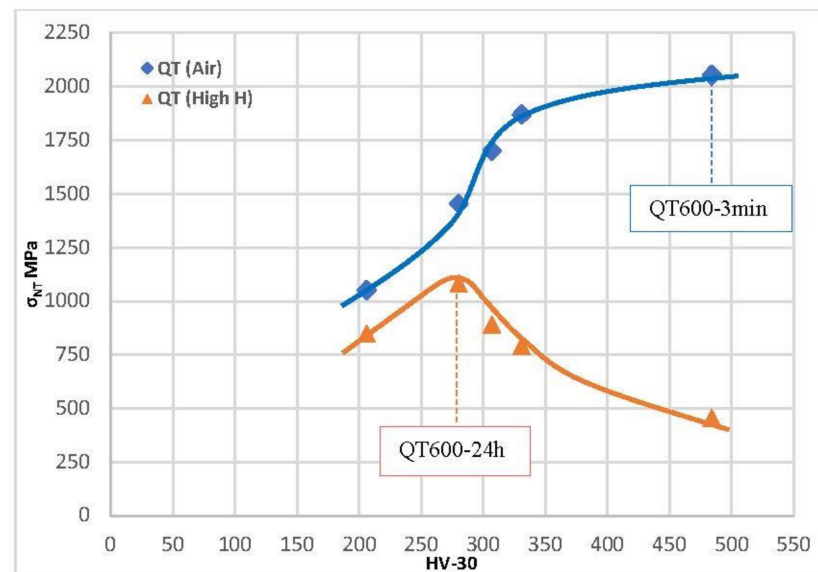


Figure 13. Notched tensile strength versus steel hardness of all quench and tempered grades tested in air and in high-H conditions.

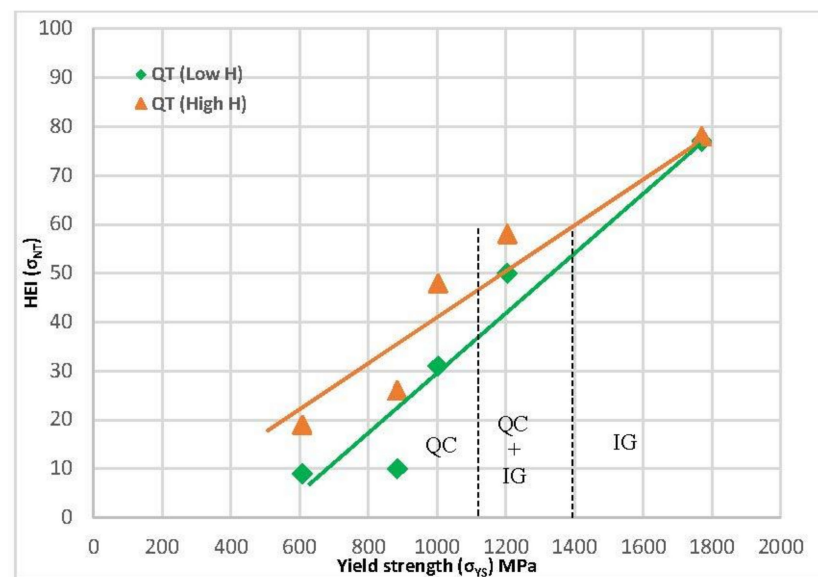


Figure 14. HEI related to notched strength vs. steel yield strength (σ_{ys}) for quenched and tempered grades tested in both hydrogenated conditions.

5. Conclusions

In situ electrochemical hydrogen-charged experiments on smooth and notched tensile specimens result in a significant intake of hydrogen. With smooth tensile specimens, embrittlement indexes related to the ultimate tensile strength in both low- and highly hydrogenated media were low, except for the grade with the highest hardness and maximum strength (tempered for 3 min at 600 °C). The grade quenched and tempered at 600 °C for 30 min had the greatest ultimate tensile strength in tests performed in both hydrogenated conditions. Hydrogen embrittlement indexes corresponding to the reduction in area show a continuous increase with the steel hardness in both hydrogenated environments. High

values, always above 60% and 70% were measured in low- and highly hydrogenated conditions, respectively.

For notched tensile specimens, the notch tip region suffers very high levels of plastic deformation and high hydrostatic stresses develop in the process zone located just ahead of the notch, where there is an important build-up of hydrogen. When evaluated in the low-hydrogenation media, notched tensile strength significantly dropped in quenched and tempered steels with a hardness over 300 HV; in the highly hydrogenated medium, notched tensile strength decreased drastically in steels with a hardness above 275 HV. In the low-hydrogenation media utilized in this experiment, QT600-2h and QT600-24h are the grades with the maximum notch tensile strength, while in the highly hydrogenated medium, QT600-24h has the highest notched strength.

The operative failure micromechanisms change from microvoids' coalescence, in all tests performed in air, to quasi-cleavage in tests with simultaneous hydrogen entrance, although intergranular failure was also observed in tests on notched tensile specimens with maximum hardness grades and maximum yield strength.

Author Contributions: Conceptualization, F.J.B.V. and A.I.; methodology, F.J.B.V.; validation, F.J.B.V. and A.I.; formal analysis, F.J.B.V.; investigation, A.I.; resources, F.J.B.V.; data curation, A.I.; writing—original draft preparation, A.I.; writing—review and editing, F.J.B.V.; visualization, A.I.; supervision, F.J.B.V.; project administration, F.J.B.V. All authors have read and agreed to the published version of the manuscript.

Funding: This research received no external funding.

Data Availability Statement: Most of the data is contained within the article. More details and materials are available on request from the corresponding author.

Conflicts of Interest: The authors declare that they have no known competing financial interests or personal relationships that could have appeared to influence the work reported in this paper.

References

1. WHO. *Fact Sheet: Ambient (Outdoor) Air Pollution*; WHO: Geneva, Switzerland, 2021.
2. Barbier, F.; Basile, A.; Nejat Veziroglu, T. *Compendium of Hydrogen Energy*; Woodhead Publishing Series in Energy; Woodhead Publishing: Sawston, UK, 2015; Volume 3. Available online: <https://shop.elsevier.com/books/compendium-of-hydrogen-energy/barbir/978-1-78242-363-8> (accessed on 18 September 2015).
3. The Future of Hydrogen, Report Prepared by the IEA for the G20, Japan. 2019. Available online: <https://www.iea.org/reports/the-future-of-hydrogen> (accessed on 1 June 2019).
4. Murakami, Y. The effect of hydrogen on fatigue properties of metals used for fuel cell system. In *Advances in Fracture Research*; Springer: Dordrecht, The Netherlands, 2007; pp. 167–195.
5. Rajabipour, A.; Melchers, R.E. Service life of corrosion pitted pipes subject to fatigue loading and hydrogen embrittlement. *Int. J. Hydrog. Energy* **2018**, *43*, 8440–8450. [[CrossRef](#)]
6. Oudriss, A.; Fleurentin, A.; Courlit, G.; Conforto, E.; Berziou, C.; Rébéré, C.; Cohendoz, S.; Sobrino, J.; Creus, J.; Feaugas, X. Consequence of the diffusive hydrogen contents on tensile properties of martensitic steel during the desorption at room temperature. *Mater. Sci. Eng. A* **2014**, *598*, 420–428. [[CrossRef](#)]
7. Murakami, Y.; Kanezaki, T.; Sofronis, P. Hydrogen embrittlement of high strength steels: Determination of the threshold stress intensity for small cracks nucleating at nonmetallic inclusions. *Eng. Fract. Mech.* **2012**, *97*, 227–243. [[CrossRef](#)]
8. Tarzimoghdam, Z.; Rohwerder, M.; Merzlikin, S.; Bashir, A.; Yedra, L.; Eswara, S.; Ponge, D.; Raabe, D. Multi-scale and spatially resolved hydrogen mapping in a Ni–Nb model alloy reveals the role of the δ phase in hydrogen embrittlement of alloy 718. *Acta Mater.* **2016**, *109*, 69–81. [[CrossRef](#)]
9. Pfeil, L.B. The effect of occluded hydrogen on the tensile strength of iron. *Proc. R. Soc. Lond. Ser. A Contain. Pap. Math. Phys. Character* **1926**, *112*, 182–195. [[CrossRef](#)]
10. Birnbaum, H.; Sofronis, P. Hydrogen-enhanced localized plasticity—A mechanism for hydrogen-related fracture. *Mater. Sci. Eng. A* **1994**, *176*, 191–202. [[CrossRef](#)]
11. Jagodzinski, Y.; Hanninen, H.; Tarasenko, O.; Smuk, S. Interaction of hydrogen with dislocation pile-ups and hydrogen induced softening of pure iron. *Scr. Mater.* **2000**, *43*, 245e51. [[CrossRef](#)]
12. Djukic, M.B.; Bakic, G.M.; Zeravcic, V.S.; Sedmak, A.; Rajcic, B. The synergistic action and interplay of hydrogen embrittlement mechanisms in steels and iron: Localized plasticity and decohesion. *Eng. Fract. Mech.* **2019**, *216*, 106528. [[CrossRef](#)]
13. Wasim, M.; Djukic, M.B.; Ngo, T.D. Influence of hydrogen-enhanced plasticity and decohesion mechanisms of hydrogen embrittlement on the fracture resistance of steel. *Eng. Fail. Anal.* **2021**, *123*, 105312. [[CrossRef](#)]

14. ANSI/CSA CHMC 1-2014; Test Method for Evaluating Material Compatibility in Compresses Hydrogen Applications—Phase I—Metals. Canadian Standards Association: Mississauga, ON, Canada, 2014. Available online: <https://www.csagroup.org/store/product/2703382/> (accessed on 1 November 2023).
15. Zhu, X.; Li, W.; Zhao, H.; Wang, L.; Jin, X. Hydrogen trapping sites and hydrogen-induced cracking in high strength quenching & partitioning (Q&P) treated steel. *Int. J. Hydrog. Energy* **2014**, *39*, 13031–13040. [[CrossRef](#)]
16. Gangloff, R.P.; Somerday, B.P. *Gaseous Hydrogen Embrittlement of Materials in Energy Technologies. The Problem, Its Characterization and Effects on Particular Alloy Classes*; Woodhead Publishing: Sawston, UK, 2012.
17. Wang, M.; Akiyama, E.; Tsuzaki, K. Effect of hydrogen on the fracture behavior of high strength steel during slow strain rate test. *Corros. Sci.* **2007**, *49*, 4081–4097. [[CrossRef](#)]
18. Zafra, A.; Peral, L.; Belzunce, J.; Rodríguez, C. Effect of hydrogen on the tensile properties of 42CrMo4 steel quenched and tempered at different temperatures. *Int. J. Hydrog. Energy* **2018**, *43*, 9068–9082. [[CrossRef](#)]
19. Zafra, A.; Álvarez, G.; Belzunce, J.; Rodríguez, C. Influence of tempering time on the fracture toughness of hydrogen pre-charged 42CrMo4 steel. *Theor. Appl. Fract. Mech.* **2022**, *117*, 103197. [[CrossRef](#)]
20. Nanninga, N.; Grochowski, J.; Heldt, L.; Rundman, K. Role of microstructure, composition and hardness in resisting hydrogen embrittlement of fastener grade steels. *Corros. Sci.* **2010**, *52*, 1237–1246. [[CrossRef](#)]
21. Ogawa, Y.; Hino, M.; Nakamura, M.; Matsunaga, H. Pearlite-driven surface-cracking and associated loss of tensile ductility in plain-carbon steels under exposure to high-pressure gaseous hydrogen. *Int. J. Hydrog. Energy* **2021**, *46*, 6945–6959. [[CrossRef](#)]
22. Imdad, A.; Arniella, V.; Zafra, A.; Belzunce, J. Tensile behaviour of 42CrMo4 steel submitted to annealed, normalized, and quench and tempering heat treatments with in-situ hydrogen charging. *Int. J. Hydrog. Energy* **2023**, *10*, 82. [[CrossRef](#)]
23. UNE-EN ISO 6892-1:2016; Metallic Materials. Tensile Test. Part 1: Test Method at Room Temperature (RT). ISO: Geneva, Switzerland, 2016.
24. Neuber, H.; Raven, F.A.; Brock, J.S. *Theory of Notch Stresses: Principles for Exact Stress Calculations*; Julius Springer: Berlin, Germany, 1937.
25. Arniella, V.; Zafra, A.; Álvarez, G.; Belzunce, J.; Rodríguez, C. Comparative study of embrittlement of quenched and tempered steels in hydrogen environments. *Int. J. Hydrog. Energy* **2022**, *47*, 17056–17068. [[CrossRef](#)]
26. Imdad, A.; Zafra, A.; Arniella, V.; Belzunce, J. Hydrogen Diffusivity in Different Microstructures of 42CrMo4 Steel. *Hydrogen* **2021**, *2*, 414–427. [[CrossRef](#)]
27. Oriani, R. The diffusion and trapping of hydrogen in steel. *Acta Met.* **1970**, *18*, 147–157. [[CrossRef](#)]
28. Zafra, A. Study on Hydrogen Diffusivity and Embrittlement of Quenched and Tempered 42CrMo4 Steel. Ph.D. Thesis, University of Oviedo, Oviedo, Spain, 2021.

Disclaimer/Publisher’s Note: The statements, opinions and data contained in all publications are solely those of the individual author(s) and contributor(s) and not of MDPI and/or the editor(s). MDPI and/or the editor(s) disclaim responsibility for any injury to people or property resulting from any ideas, methods, instructions or products referred to in the content.